
Article:
Galadzhun, I orcid.org/0000-0002-0512-3830, Capel Berdiell, I, Shahid, N orcid.org/0000-0002-8090-7619 et al. (1 more author) (2019) An Iron(II) Coordination Polymer of a Triazolyl Tris-Heterocycle Showing a Spin State Conversion Triggered by Loss of Lattice Solvent. CrystEngComm, 21 (42). pp. 6321-6504. ISSN 1466-8033

https://doi.org/10.1039/C9CE01496A

An Iron(II) Coordination Polymer of a Triazolyl *Tris*-Heterocycle Showing a Spin State Conversion Triggered by Loss of Lattice Solvent†‡

Iurii Galadzhun,[a] Izar Capel Berdiell,[a] Namrah Shahid[a] and Malcolm A. Halcrow[a,*]

Solvated crystals of "[Fe*L*$_2$][BF$_4$]$_2$·H$_2$O" (*L* = 2-(1,2,4-triazol-1-yl)-6-(pyrazol-1-yl)pyridine) contain a 1D coordination polymer, [Fe(μ-*L*)$_2${Fe(OH$_2$)$_2$*L*$_2$}][BF$_4$]$_4$. Two iron environments linked by κ^1:κ^3,μ-*L* ligands alternate in the chains, Fe(1) being coordinated by two tridentate *L* ligands and Fe(2) by four monodentate *L* and two water molecules. Fe(1) is low-spin in a freshly prepared crystal at 150 K, but gradually converts to a high-spin form when that crystal was measured at higher temperatures. Magnetic data imply this is triggered by loss of *ca* half a lattice water molecule during the experiment, rather being a thermal spin-crossover.

Spin-crossover (SCO) compounds undergo a spin state change in response to a thermal, pressure or optical stimulus.[1-3] This electronic rearrangement perturbs several physical properties at the molecular and macroscopic level including their magnetic moment, absorption spectrum and conductivity. This has led to interest in SCO materials as switching components in macro- and nano-scale devices.[4,5] Moreover, SCO is accompanied by significant structural rearrangements in a solid lattice which can involve crystallographic symmetry breaking. That can lead to hysteretic or stepwise transitions, or other forms of cooperative switching behaviour.[6] The variety of observed switching behaviours, and the number of techniques available to study them, make SCO materials a useful testbed for fundamental studies of phase transitions in molecular crystals.[7]

An important group of compounds in SCO research is iron(II) complexes of tridentate 2,6-di(pyrazol-1-yl)pyridine derivatives, of which [Fe(bpp)$_2$]$^{2+}$ is the prototype.[8] Appending tether groups or other functional substituents to the bpp framework is synthetically straightforward, and the impact of such substituents on SCO in the resultant complex is well-understood.[9] That flexibility has been exploited in ditopic "back-to-back" bpp ligands, to prepare coordination polymers or other assembly structures of [Fe(bpp)$_2$]$^{2+}$ centres.[10] However the resultant materials are often poorly crystalline, with ill-defined SCO switching properties.[11] We therefore sought other ways to link [Fe(bpp)$_2$]$^{2+}$-type centres into larger assemblies.

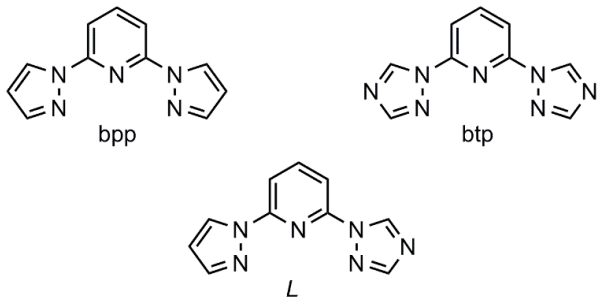

Scheme 1. The ligands described in this work.

We noted that 2,6-di(1,2,4-triazol-1-yl)pyridine (btp, Scheme 1) acts as a monodentate or *bis*-monodentate ligand to metal ions, binding through its divergent triazolyl *N*4 donor atoms.[12] Hence, we proposed the hybrid ligand 2-(1,2,4-triazol-1-yl)-6-(pyrazol-1-yl)pyridine (*L*, Scheme 1) might combine the preference of bpp for tridentate coordination, with the ability of btp to link metal ions into coordination polymers. While our work was in progress salts of mononuclear [M*L*$_2$]$^{n+}$ were reported by others,[13] which contain *L* coordinated in either tridentate (M^{n+} = Co^{2+}, Ru^{2+}) or monodentate (M^{n+} = Ag$^+$) fashion. We report here a complex of formula [Fe*L*$_2$][BF$_4$]$_2$·H$_2$O (**1**), with a more complicated structure including both of these coordination modes.

Ligand *L* was previously prepared from btp, by nucleophilic substitution of a triazolyl ring with 1 equiv sodium pyrazolate.[13] We synthesised *L* in high yields by a different nucleophilic displacement reaction, from treatment of sodium 1,2,4-triazolate with 2-fluoro-6-pyrazolylpyridine.[14] Crystal structures of both these organic compounds are in the ESI†.

[a] *School of Chemistry, University of Leeds, Woodhouse Lane, Leeds LS2 9JT, UK. Email: m.a.halcrow@leeds.ac.uk*

† Electronic Supplementary Information (ESI) available: Experimental procedures and characterisation data for the compounds in this work; crystallographic data, refinement procedures and additional Figures and tables. CCDC 1950547- 1950548 and 1951382-1951385. For ESI and crystallographic data in CIF or other electronic format see DOI: 10.1039/######.

‡ Data supporting this study are available at http://doi.org/10.5518/###.

Treatment of $Fe[BF_4]_2{\cdot}6H_2O$ with 2 equiv *L* in $MeNO_2$ affords yellow solutions, which deposit orange prisms of formula **1**$\cdot MeNO_2{\cdot}xH_2O$ ($x \approx 1.33$) upon slow diffusion of di(*iso*propyl)-ether antisolvent. The crystals degrade rapidly on exposure to air, or when stored under ether for 1-2 days, to a yellow powder analysing as solvent-free **1**. This powder in turn slowly bleaches to a white solid in air, which may indicate hydrolysis of the complex by atmospheric moisture. Hence, unless otherwise stated, all physical characterisation was undertaken using freshly prepared samples. While the crystals are well-formed they diffract weakly, which might reflect that nearly half their non-H atoms are disordered. Precise structure determinations at 150, 200, 250 and 290 K (measured in that order) were ultimately achieved, using the same very large crystal.

The structure determinations of **1**$\cdot MeNO_2{\cdot}xH_2O$ (monoclinic, *C*2/*c*) revealed that "$[FeL_2][BF_4]_2{\cdot}H_2O$" is in fact the coordination polymer $[Fe(\mu\text{-}L)_2\{Fe(OH_2)_2L_2\}][BF_4]_4$. Its asymmetric unit contains half a formula unit of the compound, with two unique iron half-atoms (Figure 1). Fe(1) lies on a crystallographic C_2 axis and binds to two tridentate *L* ligands, which also form an additional bond to Fe(2) *via* their triazolyl *N*4 donor atom. Fe(2) spans a crystallographic inversion centre and is coordinated by two bridging *L* ligands, two monodentate *L* ligands and two water molecules. While the heterocyclic rings in the bridging *L* ligand have the *cisoid* conformation required for tridentate coordination, the monodentate ligands adopt the same *transoid* conformation as metal-free *L* (Figure S4). The Fe(1) and Fe(2) centres alternate in the polymer chains, which zig-zag along the unit cell *c* axis (Figure 2).

The asymmetric unit also contains two BF_4^- ions, which are disordered at all temperatures (Figure 2); half a nitromethane molecule spanning a C_2 axis; and, an isolated Fourier peak within hydrogen bonding distance of both anions, which was treated as a partial water molecule. The occupancy of the lattice water was *ca* 0.67 in the 150 and 200 K structures, which correlates with the disorder in a neighbour anion (Figure S7). However, larger displacement parameters at higher temperatures implied a reduced occupancy for the lattice water, which was treated as 0.50-occupied at 250 K and 0.33 at 290 K (Figure S8).

Each anion hydrogen bonds to one aqua ligand and, in some of their disorder orientations, to the lattice water (Figure 2). The monodentate and bridging *L* ligands also form an interdigitated $\pi...\pi$ tetrad with another polymer chain, related by crystallographic inversion symmetry (Figure S9). These secondary interactions combine to link the polymer chains into a 3D network in the lattice (Figures S10-S11).

The pyrazolyl and pyridyl rings of the tridentate ligand were clearly disordered, and refined without restraints over two orientations (Figure 1). The refined occupancies of these sites varied slightly with temperature, from 0.621(15):0.379(15) at 150 K to 0.513(6):0.487(6) at 290 K. The disordered region of the ligand forms close van der Waals contacts to two disordered BF_4^- ions and the partial water molecule (Figure S9). Since disorder in at least one anion is also connected to the partial water occupancy (see above), all the disorder in different residues of the compound is probably inter-related.

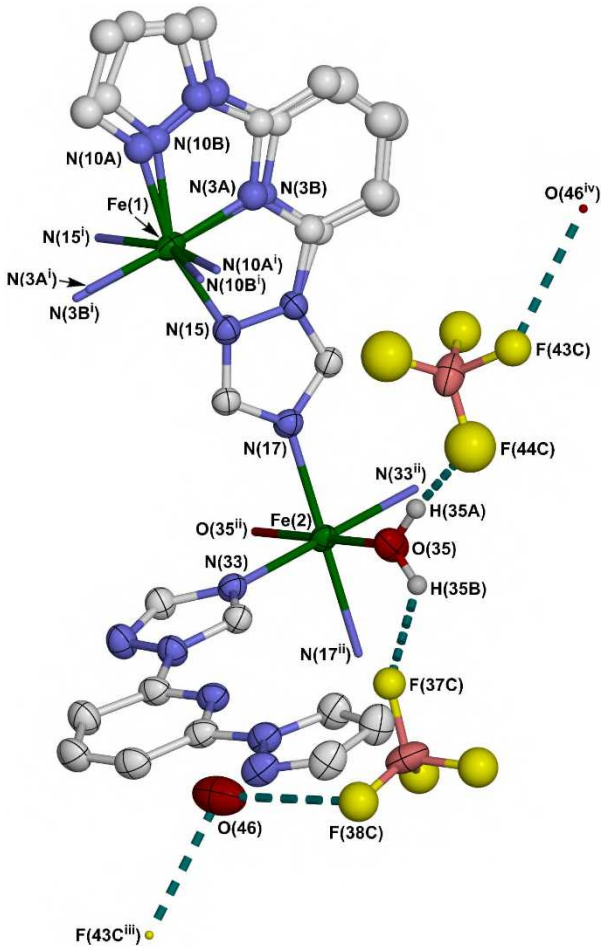

Figure 1 The asymmetric unit of **1**$\cdot MeNO_2{\cdot}xH_2O$ at 150 K, showing the ligand disorder and the hydrogen bond connectivity. For clarity only one orientation of the disordered BF_4^- ions is shown, and the $MeNO_2$ half-molecule and C-bound H atoms have been omitted. Symmetry codes: (i) 1–*x*, *y*, ½–*z*; (ii) 1–*x*, –*y*, 1–*z*; (iii) –½+*x*, –½+*y*, *z*; (iv) ½+*x*, ½+*y*, *z*. Colour code: C, white; H, pale grey; B, pink; F, yellow; Fe, green; N, blue; O, red.

The metric parameters at Fe(2) are identical at each temperature within experimental error, and are consistent with the high-spin state expected for iron(II) centre bearing two weak field aqua ligands. In contrast the Fe–N bond lengths to Fe(1) are temperature-dependent, and consistently increase at higher temperatures (Table S3). That would be consistent with a low→high-spin transition on warming, that is characteristic of a gradual thermal SCO. However, detailed consideration of the spin state of Fe(1) is complicated by its ligand disorder. It's unclear whether the A and B ligand sites can co-exist about the same Fe(1) atom, or if only 'all A' and 'all B' Fe(1) sites are present. Moreover, while Fe(1) consistently refined onto the crystallographic C_2 axis, the ligand disorder may involve unresolved displacements of Fe(1) away from that special position which would significantly affect its metric parameters. Hence, the following discussions are based on averaged structural parameters at Fe(1), calculated from all possible combinations of its two disordered ligands (Table S4).

A useful parameter in this context is V_{Oh}, the volume of the FeN_6 and FeN_4O_2 coordination octahedra at Fe(1) and Fe(2) respectively.[15] For SCO-active complexes of the $[Fe(bpp)_2]^{2+}$

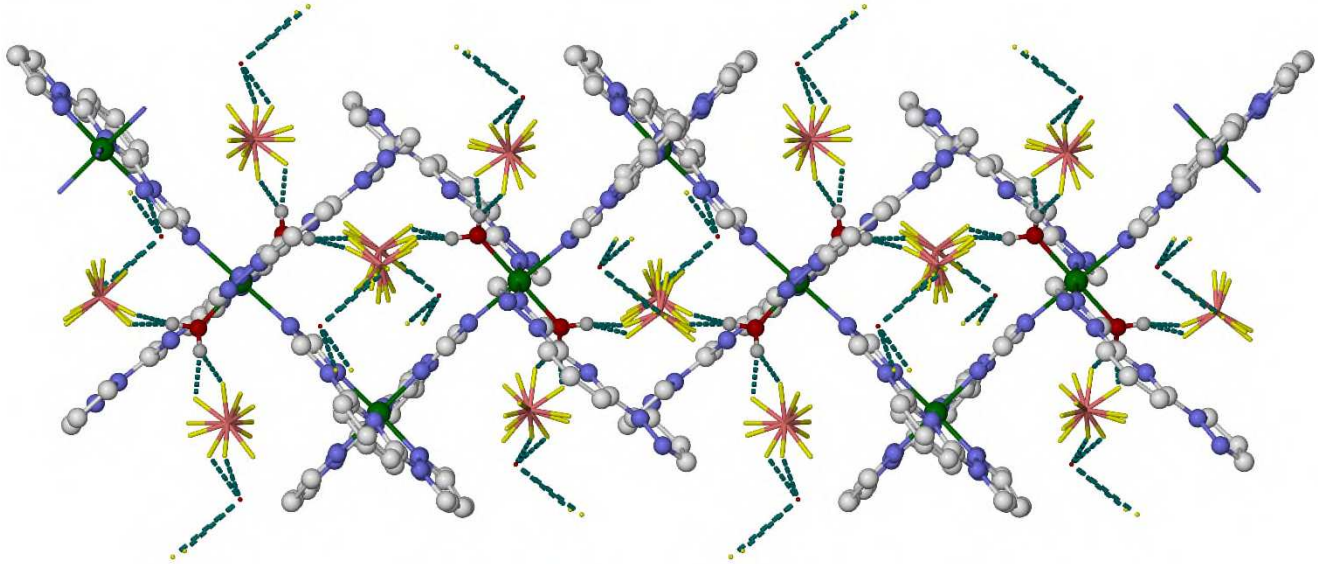

Figure 2 A coordination polymer chain in **1**·$MeNO_2$·xH_2O at 150 K. All ligand and anion disorder orientations are shown, with the anions and partial lattice water being de-emphasised for clarity. C-bound H atoms and the nitromethane solvent are not included. Colour code: C, white; H, pale grey; B, pink; F, yellow; Fe, green; N, blue; O, red.

type, V_{Oh} is typically 9.6±0.2 Å^3 for low-spin iron(II) centres and 12.6±0.2 Å^3 for their high-spin forms.[16] By that measure, Fe(2) is clearly high-spin at all temperatures examined. In contrast, Fe(1) is predominantly low-spin at 150 K, has a mixed high:low-spin population at 200 K, and is essentially high-spin at 250 and 290 K (Table 1). Ligand disorder site A has consistently shorter average Fe–N distances than site B, implying site A is more low-spin than site B at the temperatures examined (Table S3). However the parameters for both ligand sites are temperature-dependent, showing that sites A and B do not simply correspond to the low-spin and high-spin fractions of Fe(1). Rather, both ligand conformations support SCO, with site A undergoing SCO at higher temperature than site B.

Table 1 Coordination volumes of Fe(1) and Fe(2) in **1**·$MeNO_2$·xH_2O (Å^3); estimated fractional high-spin populations at each temperature; and a predicted χ_MT value based on these values (cm^{3}mol^{-1}K). V_{Oh} for Fe(1) are weighted averages of all possible values derived from different combinations of its ligand disorder sites (Table S4).

T / K	150	200	250	290
V_{Oh}{Fe(1)}	9.74(5)	10.67(5)	12.20(7)	12.24(6)
V_{Oh}{Fe(2)}	13.661(10)	13.701(11)	13.596(16)	13.628(12)
γ_{HS} {Fe(1)}[a]	0.05±0.05	0.36±0.05	0.87±0.05	0.88±0.05
γ_{HS} {Fe(2)}	1.00	1.00	1.00	1.00
Predicted $\chi_M T$[b]	3.7±0.3	4.7±0.3	6.5±0.4	6.6±0.4

[a]Estimated assuming V_{Oh} = 12.6±0.2 Å^3 for high-spin iron(II) and 9.6±0.2 Å^3 for low-spin iron(II) with this tridentate ligand geometry.[16] [b]Calculated assuming $\chi_M T$ = 3.5±0.1 cm^{3}mol^{-1}K for a high-spin iron(II) centre and $\chi_M T$ = 0 for low-spin iron(II).[17]

Magnetic susceptibility data were obtained from freshly prepared **1**·$MeNO_2$·xH_2O, which was protected from solvent loss during the measurement, and from a dried sample of solvent-free **1**. Unexpectedly, neither material showed evidence of thermal SCO by this technique (Figure 3). **1**·$MeNO_2$·xH_2O presents a constant $\chi_M T$ = 4.1 cm^{3}mol^{-1}K between 50-300 K. A high-spin iron(II) centre typically gives $\chi_M T$ ≈ 3.5 cm^{3}mol^{-1}K while low-spin iron(II) is diamagnetic.[17] By that

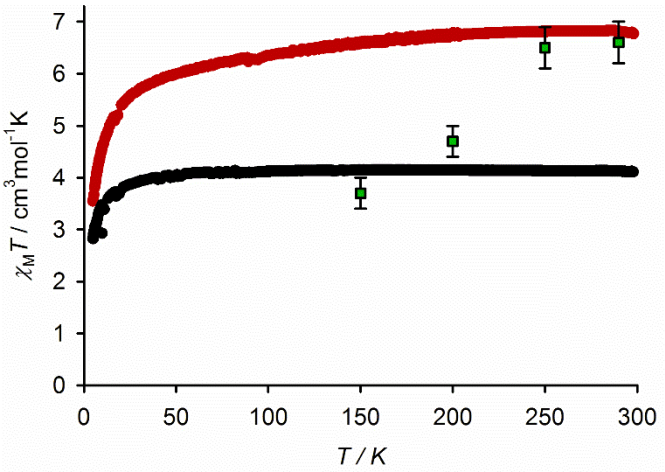

Figure 3 Variable temperature magnetic susceptibility data from **1**·$MeNO_2$·xH_2O (black) and dried **1** (red). Scan rate 5 Kmin^{-1}. The green squares show the values predicted from the crystallographic data, if the compound exhibited thermal SCO (Table 1).

measure, **1**·$MeNO_2$·xH_2O contains a high-spin Fe(2) and a constant *ca* 15 % high-spin population at Fe(1). That is close to that predicted from the 150 K structure determination (Table 1), allowing for the ambiguities of interpretation mentioned above. In contrast the dried material **1** exhibits $\chi_M T$ = 6.8 cm^{3}mol^{-1}K at room temperature. That is essentially the value expected if both iron sites are fully high-spin, as in the high-temperature crystal structures. A small decrease in $\chi_M T$ to 6.4 cm^{3}mol^{-1}K at 100 K might reflect SCO in about 10 % of the Fe(1) sites of **1** although, if so, it occurs more gradually and less completely than in the crystallographic data. Both samples show a typical reduction in $\chi_M T$ below 50 K. This is attributed to zero-field splitting of their high-spin iron(II) atoms,[18] with a smaller contribution from weak antiferromagnetic coupling between high-spin iron(II) centres *via* the μ-*L* bridging ligand.[19]

The magnetic data show the spin state properties of **1**·$MeNO_2$·xH_2O depend strongly on its lattice solvent. However

neither sample exhibits the variation in $\chi_M T$ that would be consistent with the crystallographic results (Figure 3), implying the SCO observed by crystallography is not thermally activated. We therefore propose the low→high spin state conversion at Fe(1) is triggered by the gradual loss of lattice water during sequential structure determinations from the same crystal. Loss of lattice water[20,21] or organic solvents[22] from solvated SCO materials is well known to affect their spin state behaviour, [23] by triggering significant structural rearrangements or, more often, by destroying long-range order. For example a comparable, but weaker, coupling of solvent loss to spin state occurs in an iron(II)/1,2,4-triazolate MOF material. [21]

In conclusion, our synthesis of **1** demonstrates the ability of *L* to link tridentate $[ML_2]^{2+}$ centres into larger assembly structures.[24] While the spin state of the $[FeL_2]^{2+}$ sites in **1** is temperature-dependent by crystallography this was not reproduced in the magnetic data, which did however show the spin state depends strongly on the solvation of the material. We conclude that loss of *ca* half of a two-thirds-occupied lattice water molecule during the variable temperature crystallographic study irreversibly converts **1**·$MeNO_2$·xH_2O from a low-spin to a high-spin state. Assemblies of $[FeL_2]^{2+}$ centres thus have potential to show reversible SCO switching, even though that was not observed in this case. Our current work aims to further exploit the bridging capabilities of *L*, to afford new coordination polymers or other assemblies of SCO-active $[FeL_2]^{2+}$ centres.

This work was supported by the University of Leeds, the Leverhulme Trust (RPG-2015-095) and the EPSRC (EP/N509681/1). The authors thank Dr O. Cespedes (School of Physics and Astronomy, University of Leeds) for help with the magnetic measurements.

Conflicts of interest

There are no conflicts to declare.

Notes and references

1 P. Gütlich and H. A. Goodwin (eds), *Spin Crossover in Transition Metal Compounds I–III: Topics in Current Chemistry*, Springer-Verlag: Berlin, 2004, vols. 233–235.

2 M. A. Halcrow (ed), *Spin-crossover materials – properties and applications,* John Wiley & Sons, Chichester, UK, 2013, p. 568.

3 J. Zarembowitch, F. Varret, A. Hauser, J. A. Real and K. Boukheddaden, *C. R. Chimie*, 2018, **21**, 1056.

4 K. S. Kumar and M. Ruben, *Coord. Chem. Rev.*, 2017, **346**, 176.

5 S. Rat, M. Piedrahita-Bello, L. Salmon, G. Molnár, P. Demont and A. Bousseksou, *Adv. Mater.*, *2*018, **30**, 17003862.

6 M. A. Halcrow, *Chem. Soc. Rev.*, 2011, **40**, 4119.

7 M. Chergui and E. Collet, *Chem. Rev.*, 2017, **117**, 11025.

8 L. J. Kershaw Cook, R. Mohammed, G. Sherborne, T. D. Roberts, S. Alvarez and M. A. Halcrow, *Coord. Chem. Rev.*, 2015, **289-290**, 2.

9 L. J. Kershaw Cook, R. Kulmaczewski, R. Mohammed, S. Dudley, S. A. Barrett, M. A. Little, R. J. Deeth and M. A. Halcrow, *Angew. Chem. Int. Ed.*, 2016, **55**, 4327.

10 M. Attwood and S. S. Turner, *Coord. Chem. Rev.*, 2017, **353**, 247.

11 C. Rajadurai, O. Fuhr, R. Kruk, M. Ghafari, H. Hahn and M. Ruben, *Chem. Commun.*, 2007, 2636; C. A. Tovee, C. A. Kilner, S. A. Barrett, J. A. Thomas and M. A. Halcrow, *Eur. J. Inorg. Chem.*, 2010, 1007; L. J. Kershaw Cook, J. Fisher, L. P. Harding and M. A. Halcrow, *Dalton Trans.*, 2015, **44**, 9417; A. Abhervé, M. J. Recio-Carretero, M. López-Jordá, J. M. Clemente-Juan, J. Canet-Ferrer, A. Cantarero, M. Clemente-León and E. Coronado, *Inorg. Chem.*, 2016, **55**, 9361; B. Schäfer, T. Bauer, I. Faus, J. A. Wolny, F. Dahms, O. Fuhr, S. Lebedkin, H.-C. Wille, K. Schlage, K. Chevalier, F. Rupp, R. Diller, V. Schünemann, M. M. Kappes and M. Ruben, *Dalton Trans.*, 2017, **46**, 2289.

12 See *eg* Y. Kim, S.-J. Kim and A. J. Lough, *Polyhedron*, 2001, **20**, 3073; S. J. Hong, J. Y. Ryu, J. Y. Lee, C. Kim, S.-J. Kim and Y. Kim, *Dalton Trans.*, 2004, 2697; J. Y. Ryu, J. Y. Lee, S. H. Choi, S. J. Hong, C. Kim, Y. Kim and S.-J. Kim, *Inorg. Chim. Acta*, 2005, **358**, 3398; J. Y. Ryu, J. H. Han, J. Y. Lee, S. J. Hong, S. H. Choi, C. Kim, S.-J. Kim and Y. Kim, *Inorg. Chim. Acta*, 2005, **358**, 3659; K.-T. Youm, J. Ko and M.-J. Jun, *Polyhedron*, 2006, **25**, 2318; K.-T. Youm, H. K. Woo, J. Ko and M.-J. Jun, *CrystEngComm*, 2007, **9**, 30.

13 L. J. Kershaw Cook and M. L. A. Ramsay, *Inorg. Chem. Commun.*, 2019, **104**, 207.

14 L. Wang, N. Liu and B. Dai, *RSC Adv.*, 2015, **5**, 82097.

15 P. Guionneau, M. Marchivie, G. Bravic, J.-F. Létard and D. Chasseau, *Top. Curr. Chem.*, 2004, **234**, 97.

16 I. Capel Berdiell, R. Kulmaczewski and M. A. Halcrow, *Inorg. Chem.*, 2017, **56**, 8817.

17 C. J. O'Connor, *Prog. Inorg. Chem.*, 1982, **29**, 203.

18 R. Boča, *Coord. Chem. Rev.*, 2004, **248**, 757.

19 M. B. Cingi, A. M. M. Lanfredi, A. Tiripicchio, J. P. Cornelissen, J. G. Haasnoot and J.Reedijk, *Inorg. Chim. Acta*, 1987, **127**, 189.

20 See *eg* K. H. Sugiyarto, K. Weitzner, D. C. Craig and H. A. Goodwin, *Aust. J. Chem.*, 1997, **50**, 869; M. Clemente-León, E. Coronado, M. C. Giménez-López and F. M. Romero, *Inorg. Chem.*, 2007, **46**, 11266; T. D. Roberts, F. Tuna, T. L. Malkin, C. A. Kilner and M. A. Halcrow, *Chem. Sci.*, 2012, **3**, 349; C. Bartual-Murgui, C. Codina, O. Roubeau and G. Aromí, *Chem. Eur. J.*, 2016, **22**, 12767; D. Shao, L. Shi, F.-X. Shen, X.-Q. Wei, O. Sato and X.-Y. Wang, *Inorg. Chem.*, 2019, **58**, 11589.

21 Z. Xu, W. Meng, H. Li, H. Hou and Y. Fan, *Inorg. Chem.*, 2014, **53**, 3260.

22 See *eg* M. Hostettler, K. W. Törnroos, D. Chernyshov, B. Vangdal and H.-B. Bürgi, *Angew. Chem. Int. Ed.*, 2004, **43**, 4589; J. S. Costa, S. Rodríguez-Jiménez, G. A. Craig, B. Barth, C. M. Beavers, S. J. Teat and G. Aromí, *J. Am. Chem. Soc.*, 2014, **136**, 3869; A. D. Naik, K. Robeyns, C. F. Meunier, A. F. Léonard, A. Rotaru, B. Tinant, Y. Filinchuk, B. L. Su and Y. Garcia, *Inorg. Chem.*, 2014, **53**, 1263; D. Gentili, N. Demitri, B. Schäfer, F. Liscio, I. Bergenti, G. Ruani, M. Ruben and M. Cavallini, *J. Mater. Chem. C*, 2015, **3**, 7836; R. G. Miller and S. Brooker, *Chem. Sci.*, 2016, **7**, 2501; F.-L. Yang, X. Chen, W.-H. Wu, J.-H. Zhang, X.-M. Zhao, Y.-H. Shi and F. Shen, *Dalton Trans.*, 2019, **48**, 231.

23 P. Gütlich, A. Hauser and H. Spiering, *Angew. Chem. Int. Ed.*, 1994, **33**, 2024.

24 A topologically similar coordination polymer containing $[Rh^{III}(\kappa^1{:}\kappa^3,\mu\text{-HL})_2]^+$ (H_2L = 2,6-di(benzimidazol-2-yl)pyridine) centres is described in: N. Yano, Y. Kataoka, H. Tanaka, T. Kawamoto and M. Handa, *Chem. Sel.*, 2016, **1**, 2571.